A search for systemic mass loss in Algols with bow shocks

A. Mayer[1], R. Deschamps[2, 3], and A. Jorissen[2]

[1] University of Vienna, Department of Astrophysics, Sternwartestraße 77, 1180 Wien, Austria
e-mail: a.mayer@univie.ac.at
[2] Institut d'Astronomie et d'Astrophysique, Université Libre de Bruxelles CP 226, Av. F. Roosevelt 50, B-1050 Brussels, Belgium
[3] European Southern Observatory, Alonso de Cordova 3107, Casilla 19001, Santiago, Chile

ABSTRACT

Aims. Various studies indicate that interacting binary stars of Algol type evolve non-conservatively. However, direct detection of systemic mass loss in Algols has been scarce so far. We aim at studying the systemic mass loss in Algols by looking for the presence of infrared excesses originating from the thermal emission of dust grains, which is linked to the presence of a stellar wind.
Methods. In contrast to previous studies, we make use of the fact that stellar and interstellar material is piled up at the edge of the asterosphere where the stellar wind interacts with the interstellar medium. We analyse WISE W3 $12\,\mu$m and WISE W4 $22\,\mu$m data of Algol-type binary Be and B[e] stars and the properties of their bow shocks. From the stand-off distance of the bow shock we are able to determine the mass loss rate of the binary system.
Results. Although the velocities of the stars with respect to the interstellar medium are quite low, we find bow shocks to be present in two systems, namely π Aqr, and φ Per, with a third system (CX Dra) showing a more irregular circumstellar environment morphology which might somehow be related to systemic mass-loss. The properties of the two bow shocks point to mass loss rates and wind velocities typical for (single) B stars, which do not support an enhanced systemic mass loss.

Key words. Binaries: close – Circumstellar matter – Infrared: stars – Stars: winds, outflows

1. Introduction

The group of Algols host stars with many different observed properties, like W Ser stars, β Lyræ stars, binary B[e] and Be stars, and symbiotic Algols, who all have the paradox in common that the donor star is more evolved but less massive than the accretor. This is achieved by mass transfer where the mass ratio at a certain point reverses. Non-conservative evolution in Algol type binary systems has been inferred since 60 years (Crawford 1955). For example Chaubey (1979), Sarna (1993), and van Rensbergen et al. (2011) noted that Algol models must loose a significant fraction of their mass to reproduce observed properties. One of the most efficient scenarios to remove mass from the system is via a hotspot on the surface of the gainer[1]. However, no direct detection of systemic mass loss during the mass transfer process in close binaries has been reported for Algols so far.

In this work, we focus on Be and B[e] stars for which binarity has been confirmed and the properties of the systems are well constrained. A Be star is a non-supergiant B star whose spectrum has, or had at some time, one or more Balmer lines in emission, and might also show infrared (IR) excess (Collins 1987). The origin of these spectral features in these binary Be stars is probably linked to the mass-transfer event (Porter & Rivinius 2003). The IR excess is most likely caused by hot circumstellar dust (Lamers et al. 1998), which is in case of an evolved binary system associated with mass transfer events (e.g., Dunstall et al. 2012). B[e] stars have additionally also strong forbidden (Fe) emission lines.

We take advantage of the fact that some of these stars are not at rest but move with a certain speed with respect to their surrounding medium. Assuming that mass is expelled supersonically from the binary system, it is decelerated by the oncoming interstellar medium (ISM), forming a bow shock (Baranov et al. 1971; Weaver et al. 1977). Bow shocks have been observed at all kinds of wavelengths around many stellar types, covering runaway O stars to AGB stars (e.g., van Buren & McCray 1988; Cox et al. 2012). In the mid-IR, those shocks are visible through thermal dust emission, when the shock front heats up dust grains at the interface between the stellar wind and the ISM (Ueta et al. 2006). A bow shock detection around an Algol is therefore a direct evidence for stellar material around the binary system. In this case, the distance of the system to the apex of the bow shock can be used to derive the systemic mass loss rate, if the wind velocity, stellar velocity, and ISM density are known (Baranov et al. 1971).

This research note is a complementary study to the work done by Deschamps et al. (2015, named D15 hereafter), but emphasizing on the observational aspects of the systemic mass loss. Based on radiative transfer calculations, Deschamps et al. (2015, their Fig. 13) predicted the IR colour excesses expected in the case of systemic mass loss. Additionally to the WISE detections of extended material around CZ Vel and SX Aur presented in D15, we discuss the properties of the circumstellar emission of three other objects, namely CX Dra, π Aqr, and φ Per.

2. WISE observations

In D15, we performed a systematic search for extended IR emission around Algols (collected from the catalogues of Brancewicz & Dworak 1980, and Budding et al. 2004) and Algol-related Be
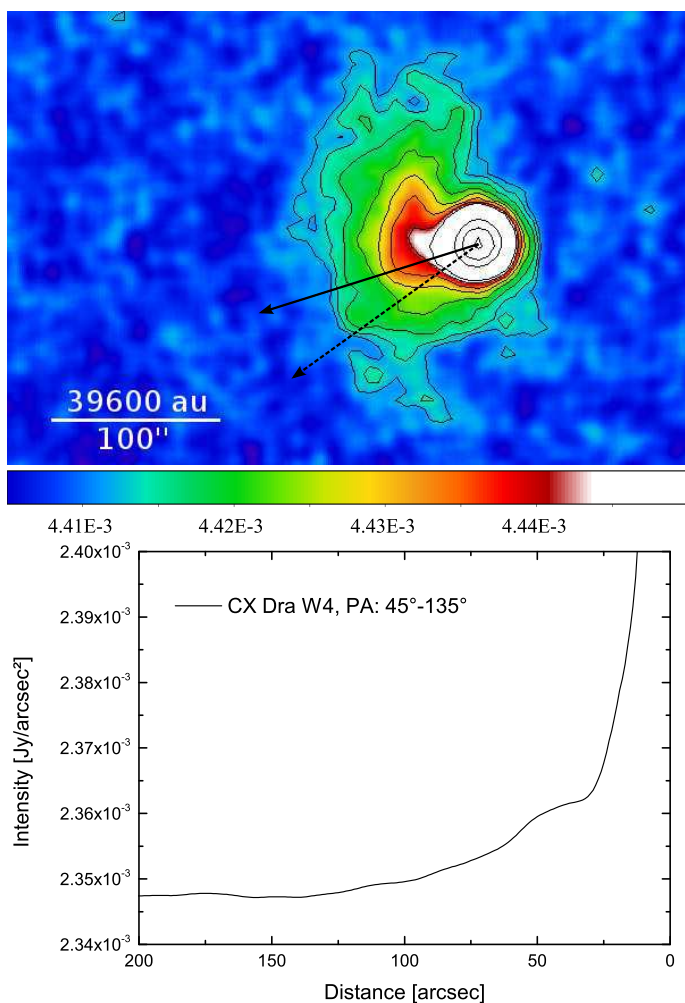
---

[1] for an extensive explanation of the hotspot mechanism, see van Rensbergen et al. (2011) and Deschamps et al. (2013, 2015).

Fig. 1. *Upper panel*: WISE W4 image of CX Dra at $22\,\mu$m. The continuous black arrow gives the uncorrected proper motion from the reprocessed Hipparcos catalogue (van Leeuwen 2007), while the dashed arrow points to the direction of the space motion corrected from the solar motion (Coşkunoğlu et al. 2011). The values of the motion are given in Tab. 1. The values of the colour bar are given in Jy pix^{-1}. *Lower panel*: Integrated intensity cut through a wedge covering position angles (P.A.): 45°–135°.

and B[e] systems (Harmanec 2001), using archive data from the Wide-field Infrared Survey Explorer (WISE)[2]. WISE is an all-sky survey, which mapped the sky in four bands at 3.4, 4.6, 12, and $22\,\mu$m with angular resolutions of 6''1, 6''4, 6''5, and 12''0, respectively (Wright et al. 2010). Based on the list of 70 objects (Algols and Algol-like Be stars with a WISE-source counterpart) provided by D15[3], we found three systems, CX Dra, π Aqr, and φ Per, to have unambiguous circumstellar emission and which therefore deserve a specific analysis (besides CZ Vel and SX Aur already discussed in D15).

All three objects are in the list of binary Be stars compiled by Harmanec (2001). They exhibit peculiarities that flag them as Algol candidates, or at least as systems with on-going mass transfer. With its sdO companion, φ Per has obviously undergone a severe mass transfer, the primary, more luminous B2[e] component being the most massive but the least evolved. In CX Dra, mass transfer in the binary has been inferred from the varia-

---

[2] The IRSA:WISE archive can be found at http://irsa.ipac.caltech.edu/applications/wise/
[3] the list of objects can be found in Appendix A

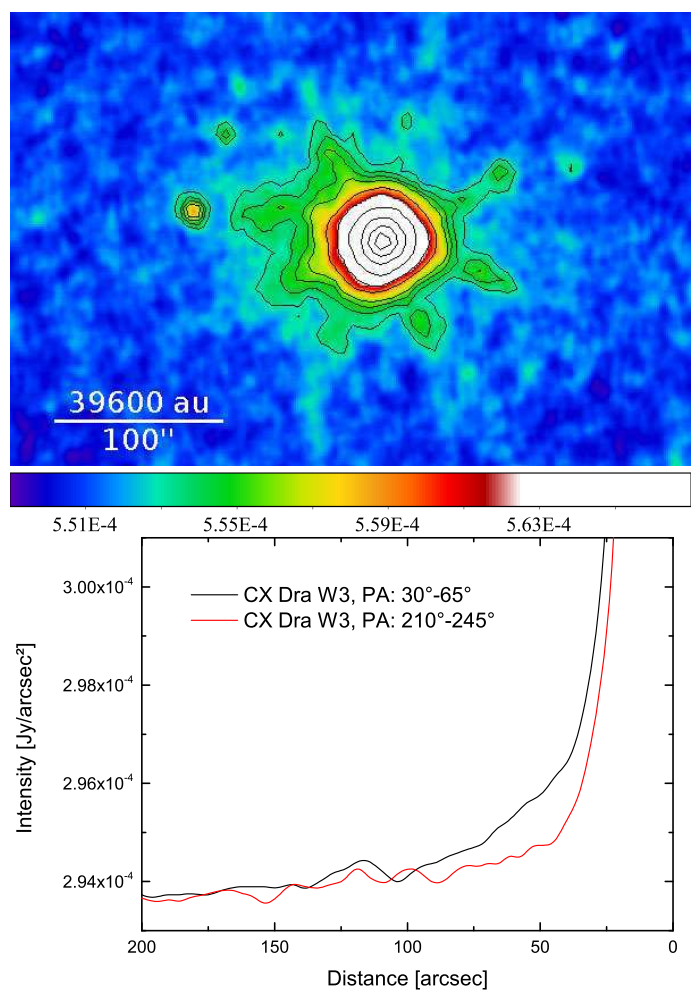**Fig. 2.** *Upper panel*: WISE W3 images of CX Dra at $12\,\mu$m. *Lower panel*: Integrated intensity cuts through a wedge covering P.A.: 30°–65° (black line) where emission is visible and P.A.: 210°–245° (red line) without extended emission. We had to choose smaller wedges to avoid that the flux be dominated by the diffraction spikes of the PSF.

tion of the polarisation with orbital phase, and from the fact that the least massive, more evolved F5III companion fills its Roche lobe (Berdyugin & Piirola 2002). In π Aqr, photometric, spectroscopic (broad and complex Hα line profile), and polarimetric variations observed during the second half of the 20th century are tentatively attributed to variable mass transfer between the binary components (Bjorkman et al. 2002; Hanuschik et al. 1996).

The extended emission around the stars was detected in Band 3 (W3) at $12\,\mu$m (CX Dra, π Aqr) and Band 4 (W4) at $22\,\mu$m (CX Dra, π Aqr, φ Per). For the two objects with circumstellar emission (CSE) detected in both bands, WISE W4 offers greater details, most likely because the thermal emission of the (shock-heated) dust grains peaks at longer wavelengths (Draine 1981). In the following, the CSM morphology of the three objects is described. Figures 1–5 depict the WISE images of CX Dra, π Aqr, and φ Per, while Tab. 1 provides their stellar properties.

2.1. CX Dra

CX Dra (HIP 92133) is a 6.696 d period Algol B2.5Ve+F5III system at a distance of 396 pc (van Leeuwen 2007) with one
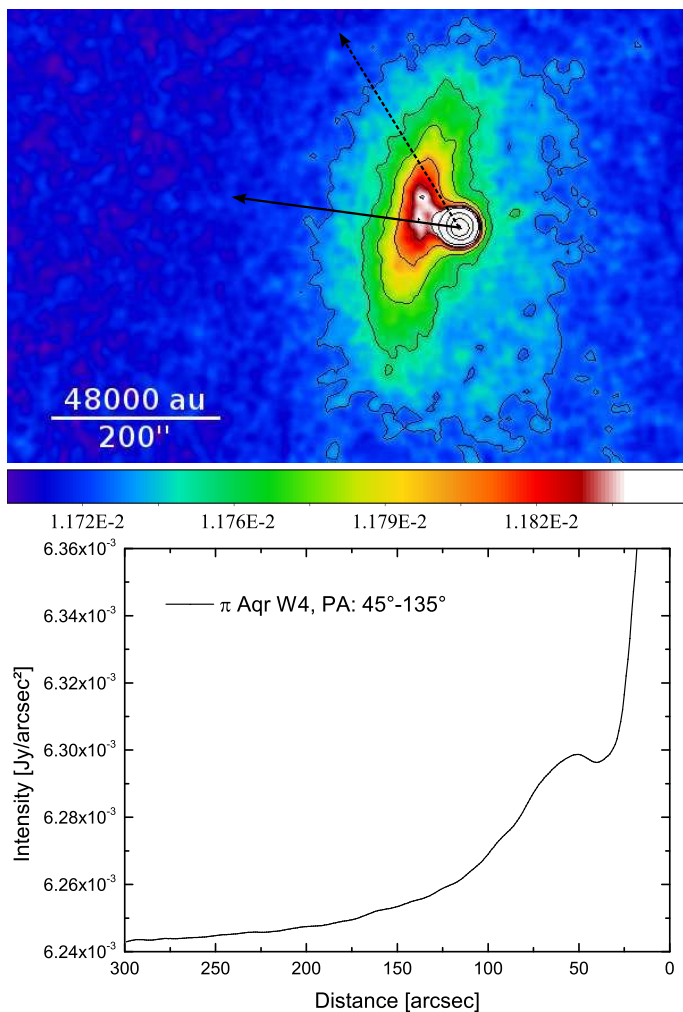
Fig. 3. Same as Fig. 1 for π Aqr. The integrated intensity cut in the lower panel covers PA: 45°–135°.

Fig. 4. Same as Fig. 2 for π Aqr at $12\,\mu$m. The integrated intensity cuts in the lower panel cover P.A.: 30°–65° (black line) where emission is visible and P.A.: 210°–245° (red line) without extended emission.

of the component rapidly rotating. Despite not being eclipsing, Berdyugin & Piirola (2002) estimate the mass of the two components to be 3.9 $M_\odot$ and 0.9 $M_\odot$ at $i = 70°$. The authors, however, correctly remark that these masses are too small to match the spectral types of both stars.

The circumstellar environment of the star is shown in Figs. 1 and 2. The emission in the WISE W4 $22\,\mu$m band is concentrated to the east of the star and traceable to a distance of about 120″ (47 500 au at 396 pc). The morphology of the circumstellar material is somewhat puzzling because several aspects are not in favour of an ISM interaction. First, the direction of the proper motion is S-E but the shape of the emission is not symmetric and more concentrated N-E of the star. Second, the emission is not detached from the star and the flux seems to decrease with distance, which is not to be expected for a bow shock where the brightest region is at the position of the shock front.

Furthermore, the circumstellar material of CX Dra on the WISE image describes an arc emerging east of the star and curved towards the north. Similar arcs are found to be part of an Archimedean spiral which is caused by a (semi-) detached companion interacting with the wind of a primary (e.g. Mastrodemos & Morris 1999; Mayer et al. 2011; Maercker et al. 2012). The spacing of the spiral arms is thereby defined by the wind velocity of the mass losing star and the orbital period of the companion. However, assuming a wind velocity of $1000\,\mathrm{km\,s^{-1}}$
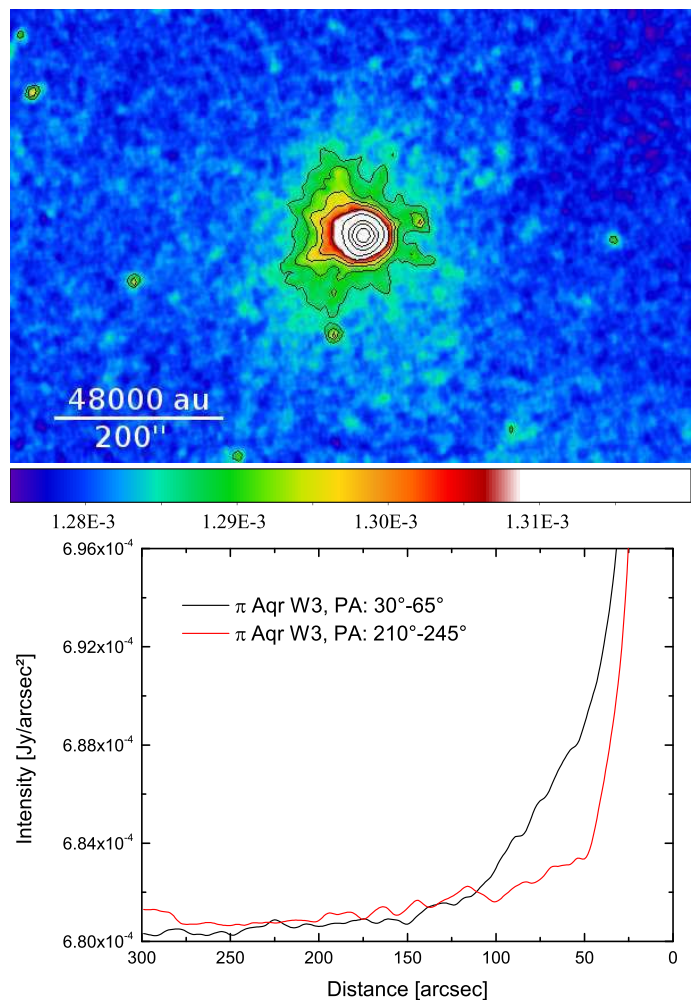
for the B2.5Ve star and an orbital period of 6.696 d for the F5III companion, the resulting spiral spacing is 3.87 au, which is several orders of magnitude smaller than what is seen on the WISE image. For comparison, the pixel size of the image is 1″375, which is 545 au at 396 pc. This implies that a spiral formed by the B2.5Ve+F5III system would show 140 windings per WISE W4 pixel. The observed arc is therefore not related to this shaping mechanism.

In the colour-colour diagram shown in Fig. 13 of D15, depicting the WISE W4/W1 against 2MASS J/K_s flux ratios, CX Dra is located only slightly above the black body curve (F_J/F_{K_s}=1.678, F_{W4}/F_{W1}=0.047). Many other objects fall into this region of the diagram and no peculiarity can be drawn from it. Still, there is no doubt that extended emission is present from the WISE W4 image.

In the shorter WISE W3 band at $12\,\mu$m (see Fig. 2), CX Dra also shows extended emission east of the star but in much less detail than in the W4 image. The detection of emission in W3 and W4, however, allow us to estimate the temperature of the dust emission around CX Dra. We performed aperture photometry on a circle of radius 15″ in both bands. The region we chose is centred at a distance of 56″ from the star at PA = 48° and falls between the diffraction spikes of the PSF which is dominating the W3 image. The resulting fluxes are $F_{\nu,12} = 0.207\,\mathrm{Jy}$ and $F_{\nu,22} = 1.650\,\mathrm{Jy}$ at $12\,\mu$m and $22\,\mu$m, respectively. Adopting
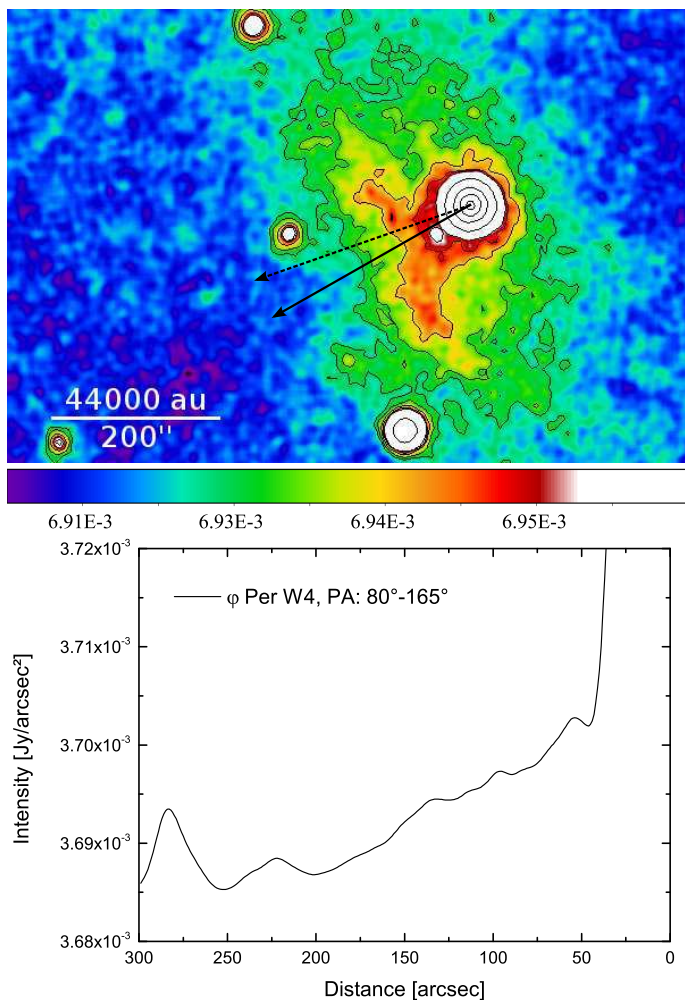
Fig. 5. Same as Fig. 1 for φ Per. The integrated intensity cut in the lower panel covers P.A.: 80°–165°. The peaks at distances of about 223″ and 283″ on the lower panel correspond to the stars visible on the image at position angles of 99° and 164°, respectively.

the corresponding absorption coefficients of astronomical silicates $Q_{\mathrm{abs},12} = 5.60 \times 10^{-2}$ and $Q_{\mathrm{abs},22} = 3.39 \times 10^{-2}$ (Draine 1985), the $12\,\mu$m and $22\,\mu$m fluxes correspond to a temperature of 124 K (for details see Jorissen et al. 2011).

Since no other archival observations are available for CX Dra, we cannot conclude on the shaping mechanism of its circumstellar material. However, we want to remark that the star might be a possible candidate for showing systemic mass loss in its circumstellar environment but further observations are needed.

2.2. π Aqr

π Aqr (HIP 110672) is a 84.1 d period binary located 240 pc away from the sun (van Leeuwen 2007). The system comprises a rapidly rotating B1Ve star at the origin of the Be phenomenon and an A-F type companion. Bjorkman et al. (2002) estimate the mass of the components to be $M_1 \sin^3 i = 12.4\,M_\odot$ and $M_2 \sin^3 i = 2.0\,M_\odot$ with an orbital inclination $i = (50-75)°$. The stellar wind is one of the fastest among Be stars with a terminal velocity of $1450\,\mathrm{km\,s^{-1}}$ and the mass-loss rate one of the largest with $\dot{M} = 2.61 \times 10^{-9}\,M_\odot\,\mathrm{yr^{-1}}$ estimated from the Si IV profile (Snow 1981). We note that the Si IV lines are likely to form inside

the Roche lobe of the gainer star and might therefore not trace the systemic mass loss rate.

The WISE W4 image of π Aqr is depicted in Fig. 3. The emission shows a morphology that is typical for a wind-ISM interaction with a bow shock in the direction of the space motion. The bow shock cone is quite symmetric on the northern and southern half, extending to about 220″ (52 800 au at 240 pc) in those directions. In the direction of motion, the material can be traced to about 150″ (36 000 au) from the binary system. The emission peak, however, is closer to the system at about 52″ (12 480 au).

In WISE W3 at $12\,\mu$m (see Fig. 4), the CSE is concentrated to the east of the star, at the same position where the bow shock in W4 is visible, but not as extended in north-south direction. The lower panel of Fig. 4 shows cuts through regions with and without extended emission.

In the same manner as for CX Dra, we performed aperture photometry ($r = 15″$) also for π Aqr in both bands at a region centred at a distance of 61″ from the star at PA = 46°. The resulting fluxes are $F_{\nu,12} = 0.481$ Jy and $F_{\nu,22} = 4.411$ Jy at $12\,\mu$m and $22\,\mu$m, respectively. Adopting the same absorption coefficients of astronomical silicates as for CX Dra, the $12\,\mu$m and $22\,\mu$m fluxes correspond to a temperature of 120 K.

2.3. φ Per

φ Per (HIP 8068) is a long period Algol B2[e]+sdO system ($P_{\mathrm{orb}} = 127$ d) at a distance of 220 pc (van Leeuwen 2007). The system is likely at the end of its mass-transfer phase (Gies et al. 1998) and the material transferred from the donor star largely spun up the gainer star (primary) to the rotation rate now observed. Based on double-line spectroscopic orbital elements, the masses of the components have been estimated to be 9.3±0.3 $M_\odot$ for the B[e] primary and 1.14 ± 0.04 $M_\odot$ for the sdO secondary (donor star). A hotspot region detected on the edge of the disc produces strong Fe IV lines. The envelope of the companion has mostly been stripped off by the Roche-lobe overflow (RLOF) event and the secondary, now a hot sdO star, is only visible in the UV.

The WISE W4 $22\,\mu$m emission of φ Per is shown in Fig. 5. The CSM is elliptically shaped with the major axis approximately in the N-S direction. The extent of the emission to the south is about 290″ (63 800 au at 220 pc) while the frame is cut-off in the north 250″ from the star. East of the star, at $\approx 100″$ (22 000 au), a brightened bar is visible with the same N-S orientation as the whole elliptical emission and a length of about 240″ (52 800 au). The bar is bent towards the star at the same position angle as the direction of the space motion, which indicates that this is the interface where the ISM interacts with the stellar material. Such bending are visible in hydrodynamic simulations of bow shocks where the shocked stellar and ambient material cool efficiently (see Fig. 15 of Comeron & Kaper 1998). A beautiful observed example of such a bended bow shock is found around the AGB star X Her (Jorissen et al. 2011). In contrast to the other two objects, φ Per does not show extended emission in WISE W3.

3. Bow shock properties and systemic mass loss

For a star which moves with respect to its surrounding medium, the stellar motion adds an asymmetry to the wind velocity profile, since different parts of the wind face the ISM with different relative velocities. If the motion is supersonic, a bow shock arises

Table 1. Stellar properties. The space velocities were calculated following Johnson & Soderblom (1987) using the Hipparcos proper motion and parallax (van Leeuwen 2007) and radial velocities from the catalogue by de Bruijne & Eilers (2012). The adopted solar motion to convert heliocentric motion into LSR motion is $(U, V, W) = (8.50 \pm 0.29, 13.38 \pm 0.43, 6.49 \pm 0.26)$ km s^{-1} (Coşkunoğlu et al. 2011).

	CX Dra	π Aqr	φ Per
Spec. type	B2.5Ve+F5III	B1Ve+[A-F]	B2[e]+sdO
M_1 [$M_\odot$]	3.9	14.0 ± 1.0	9.3 ± 0.3
M_2 [$M_\odot$]	0.9	2.3	1.1 ± 0.1
$P_{\rm orb}$ [d]	6.696	84.1	127
D [pc]	396 ± 35	240 ± 15	220 ± 9
z [pc]	149	169	43
$n_{\rm H}$ [cm^{-3}]	0.45	0.37	1.30
RV [km/s]	-2.1 ± 2.3	-4.9 ± 0.1	-4.0 ± 2.1
v_* [km/s]	21.1 ± 2.0	21.0 ± 1.1	29.8 ± 1.6
P.A. [°]	107.6 ± 1.2	82.3 ± 0.6	119.7 ± 0.2
i [°]	-5.7 ± 63.1	-13.5 ± 1.2	-7.7 ± 30.3
$v_{*,\rm LSR}$ [km/s]	25.5 ± 2.1	13.5 ± 1.0	13.1 ± 1.7
P.A.$_{\rm LSR}$ [°]	125.7 ± 1.0	31.5 ± 0.5	109.4 ± 0.6
$i_{\rm LSR}$ [°]	32.4 ± 11.4	6.6 ± 3.7	-4.4 ± 90
Ref.	1	2,3,4	5

References. (1) Berdyugin & Piirola (2002); (2) Zharikov et al. (2013); (3) Linnell et al. (1988); (4) Bjorkman et al. (2002); (5) Hummel & Štefl (2001)

at the interface where the ram pressure of the ISM and the stellar wind balance. The stand-off distance, i.e. the distance of the star to the apex of the shock front, is given by:

$$R_0 = \sqrt{\frac{\dot{M} v_w}{4\pi \rho_0 v_*^2}}, \tag{1}$$

where v_w is the terminal wind velocity, v_* the stellar velocity with respect to the ISM, $\dot{M}$ the mass loss rate, and ρ_0 the density of the surrounding medium (Baranov et al. 1971). The density can be expressed in a number density of hydrogen atoms ($m_{\rm H} = 1.6727 \times 10^{-27}$ kg), which follows roughly

$$n_{\rm H} = 2.0 \, e^{-\frac{|z|}{100\,\rm pc}}, \tag{2}$$

where z is the galactic height (Mihalas & Binney 1981) and $n_{\rm H}$ is given in atoms per cm^3. Wilkin (1996) demonstrated that the shape of the bow shock only depends on the stand-off distance, while Cox et al. (2012) showed that this assumption remains valid for viewing angles up to 70°. Above this value, the bow shock cone becomes broader. Therefore, we could use Eq. 1 to estimate the mass loss rate from the binary system by measuring the stand-off distance. Generally, the ISM density and stellar velocity can be determined following Eq. 2 and Johnson & Soderblom (1987), respectively. While the error of the space motion is negligible, the ISM density value is only an estimate since the star could move through a dense cloud which is not considered by Eq. 2. The respective values of these quantities for the three objects are given in Tab. 1. To obtain the space motion ($v_{*,\rm LSR}$) with respect to the Local Standard of Rest, we corrected the heliocentric motions from the solar motion vector $(U, V, W)_\odot = (8.50 \pm 0.29, 13.38 \pm 0.43, 6.49 \pm 0.26)$ km s^{-1} (Coşkunoğlu et al. 2011). However, since the proper motions are quite small (a few mas yr^{-1}), the correction for the solar motion has a large impact, especially on the P.A. of the motion. Interestingly, the P.A. of the corrected LSR motion is a worse
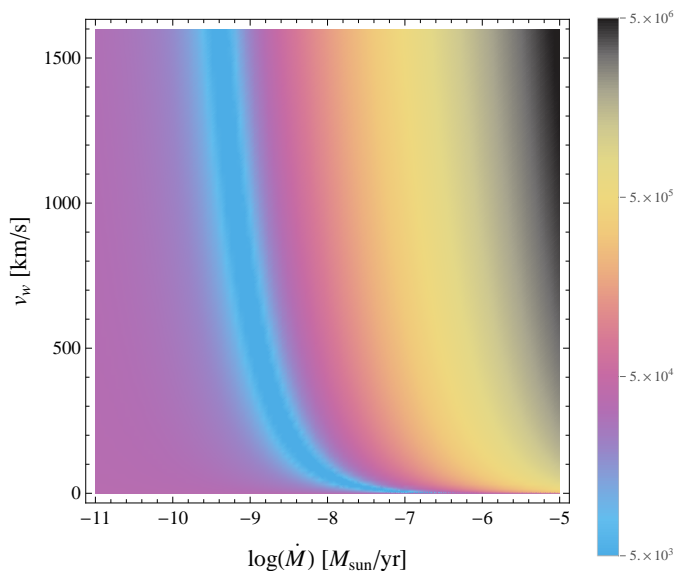

Fig. 6. Density plot relating the mass loss rate and wind velocity of π Aqr to the bow-shock stand-off distance R_0. The colours indicate the difference in au to the measured $R_0 = 36\,000$ au.

match to the bow-shock orientation than the P.A. of the uncorrected motion (see Figs. 1, 3, 5). Using $(U, V, W)_\odot = (10.00 \pm 0.36, 5.25 \pm 0.62, 7.17 \pm 0.38)$ km s^{-1} determined from Hipparcos data by Dehnen & Binney (1998) leads to $v_{\rm LSR}$ velocities which are slightly closer to the better-matching heliocentric values. A similar discrepancy between bow-shock orientation and LSR motion (and less so with heliocentric motion) is found by Peri et al. (2012, 2015) for a large number of O and B-type stars with bow shocks, as collected in the WISE E-BOSS survey. For this reason, we over-plotted both the heliocentric and LSR motions on the WISE images in Figs. 1, 3, 5.

Sarna (1993), van Rensbergen et al. (2011), and more recently Deschamps et al. (2013, 2015) suggested that Algols lose a significant fraction of their initial mass during the mass-transfer phase. van Rensbergen et al. (2011) state that a hotspot mechanism may be invoked to remove up to 15% of the binary-system initial mass. In this scenario, those parts of the stellar surface impacted by the RLOF stream (the hotspot) emit radiation whose pressure triggers mass loss, at a rate of up to 10^{-5} $M_\odot$ yr^{-1}. Such a high mass loss rate would change the size of the bow shock massively. Moreover, a stream winding around the binary system forms (see Fig. 1 of D15), possibly altering as well the shape of the bow shock.

In order to identify the origin of the mass causing the observed bow shocks, one has to evaluate the dynamical age of the bow shock. The distance of the bow shocks to the central system is 22 000 au and 36 000 au for φ Per and π Aqr, respectively. If the bow shocks are caused by systemic mass loss triggered by a hot spot, the wind velocity is about 1000 km s^{-1} (see Fig. 3 of D15), and the resulting kinematic ages of the bow shocks are of the order of 100 yr, much shorter than the duration of the mass-transfer phase in Algol systems (10^5 yr; Deschamps et al. 2013). Therefore, for Algols currently in the rapid mass-transfer phase, if a bow shock is present, it will stay for the whole duration of the mass transfer.

Since the wind velocities of π Aqr and φ Per are not known, we cannot directly use Eq. 1 to relate the bow-shock stand-off distance to the mass-loss rate causing the bow shock, and then
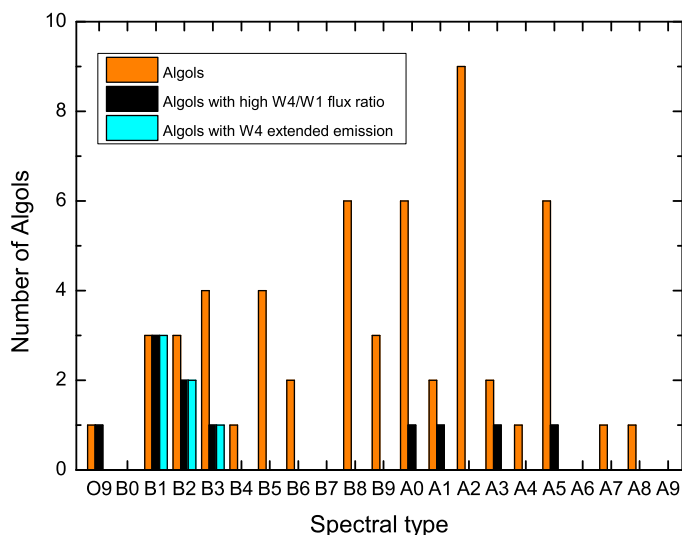
Fig. 7. Distribution of Algols among early spectral types (orange bars), along with those with detected extended emission in the WISE W4 band (cyan bars) and with W4/W1 flux ratios falling above the black body line (black bars).
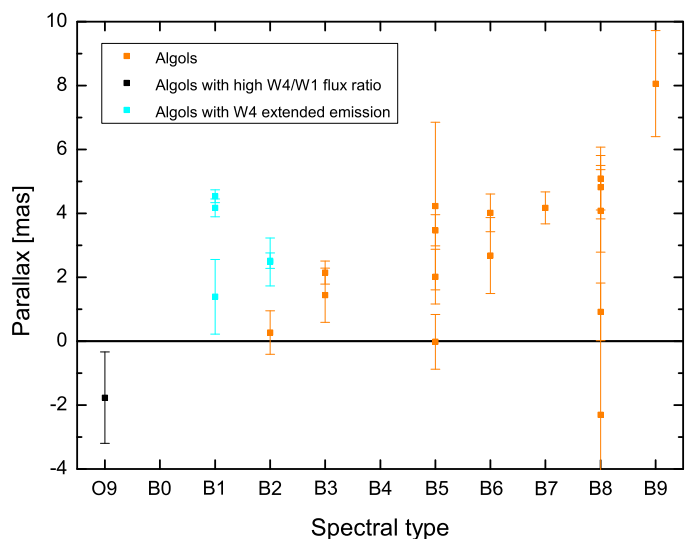

Fig. 8. Distance distribution of Algols earlier than spectral type A. Orange squares are Algols without detection of circumstellar material, cyan squares show those with detected extended emission in the WISE W4 band, and black squares those with W4/W1 flux ratios falling above the black body line (according to Fig. 13 of D15).

compare the latter with the predictions of systemic mass-loss rates from the hotspot scenario of D15. Nevertheless, the relation between the mass-loss rate and the wind velocity may help us to evaluate the likelihood of systemic mass loss triggered by the hotspot scenario. In these calculations, we used the ISM densities $\rho_0 = n_H \times m_H$ and space velocities $v_{*,\mathrm{LSR}}$ listed in Table 1 with stand-off distances of $R_0 = 36\,000$ au for π Aqr and $R_0 = 22\,000$ au for φ Per, as measured on the WISE images. Fig. 6 depicts the relationship between mass-loss rate and wind velocity for π Aqr. The colour codes the difference of the calculated R_0 to the observed value of 36 000 au.

For an expected wind velocity between 700 and 1500 km s^{-1}, only a small range of mass-loss rates of order of $4 \times 10^{-10}\,M_\odot$ yr^{-1} to $4\times10^{-9}\,M_\odot$ yr^{-1} can match the observed stand-off distance (±5000 au) of the bow shock around π Aqr. This range of mass-loss rates is well below the systemic mass-loss rate inferred from the hotspot scenario (of the order $10^{-5}\,M_\odot$ yr^{-1}). Such a high mass-loss rate, in combination with a wind velocity of ≈ 1000 km s^{-1}, would cause a stand-off distance which is a factor 100 larger than observed. To bring the wind velocity in line with the proposed $\dot{M}$ from the hotspot scenario and with the observed R_0, it has to decrease almost to 0. In other words, it is highly unlikely that a systemic mass loss of order of $10^{-5}\,M_\odot$ yr^{-1} is currently present in π Aqr. If systemic mass loss is ongoing, it does not exceed $10^{-8}\,M_\odot$ yr^{-1}. We stress, however, that the mass-loss rate of π Aqr inferred from the bow-shock properties fits well the value observed for the Be star ($2.61 \times 10^{-9}\,M_\odot$ yr^{-1}; Snow 1981). For φ Per, we obtain similar results: $\dot{M} = 2 \times 10^{-10} - 6 \times 10^{-9}\,M_\odot$ yr^{-1} for v_w =700–1500 km s^{-1} for a measured R_0 of $22\,000 \pm 5000$ au.

The Be star wind as the origin of the bow shock is further demonstrated by the fact that the bow shocks discovered in the present study are restricted to early-type B stars (Figs. 7–8). Our sample includes also a O9.7Ibe star, RY Sct, which shows a high WISE W4/W1 flux ratio. However, RY Sct is much further away than the three B stars discussed in the present paper, since it has a parallax non significantly different from zero (van Leeuwen 2007); hence, if present, the extended emission would be hardly detectable. Given that the V magnitude of RY Sct (O9.7Ibe) amounts to 9.1, as compared to $V = 4.6$ for π Aqr (B1Ve),

RY Sct is located at least a factor of 10 farther away than π Aqr. All other parameters being equal, the bow shock of RY Sct would thus extend up to $15''$ only from the star, and would not be resolved by WISE. This conclusion is supported by Fig. 8 which reveals that the Be stars with a detected bow shock are the nearest and the warmest of the sample.

The second Be star with extended emission we did not include in this study is the B2Vne star V696 Mon. The WISE W4 image is depicted in the upper panel of Fig. 9 and shows a peculiar morphology around the star. The extended emission reaches north of V696 Mon and seems to engulf the star BD -06°1393 located $148''$ away from V696 Mon at PA = 8°. This association is probably not real, since the Tycho-1 parallaxes of the two stars are quite different. Although the space velocity of V696 Mon $[v_{*,\mathrm{LSR}} = (15.8 \pm 6.2)\,$km s$^{-1}]$ is comparable to the three stars studied here and the IR emission seems to be aligned with the direction of the space motion, the upstream structure does not resemble a bow shock.

We also want to remark that the surrounding ISM of V696 Mon is extremely rich (the star-forming region Monoceros R2 is located $56'$ away) as seen in the IRAS 100 μm image (lower panel of Fig. 9), and it is difficult to conclude whether the WISE 22 μm emission originates from CSM or ISM.

4. Conclusion

We studied a sample of 70 Algol and Algol-like Be systems with entries in the WISE catalogue[4] with the aim of identifying those Algol systems surrounded by dust left over by systemic mass loss. In D15, the two objects, CZ Vel and SX Aur, were discussed, and here, we found three new objects, CX Dra, π Aqr, φ Per, to show circumstellar material in the WISE W4 band at 22 μm and for π Aqr and CX Dra also in WISE W3 at 12 μm. The two objects π Aqr and φ Per show clear evidence for an interaction of circumstellar material with the ISM.

---

[4] We checked as well the Herschel Science Archive, but only two of the 70 targets were observed by the Herschel Space Observatory, none showing circumstellar emission.
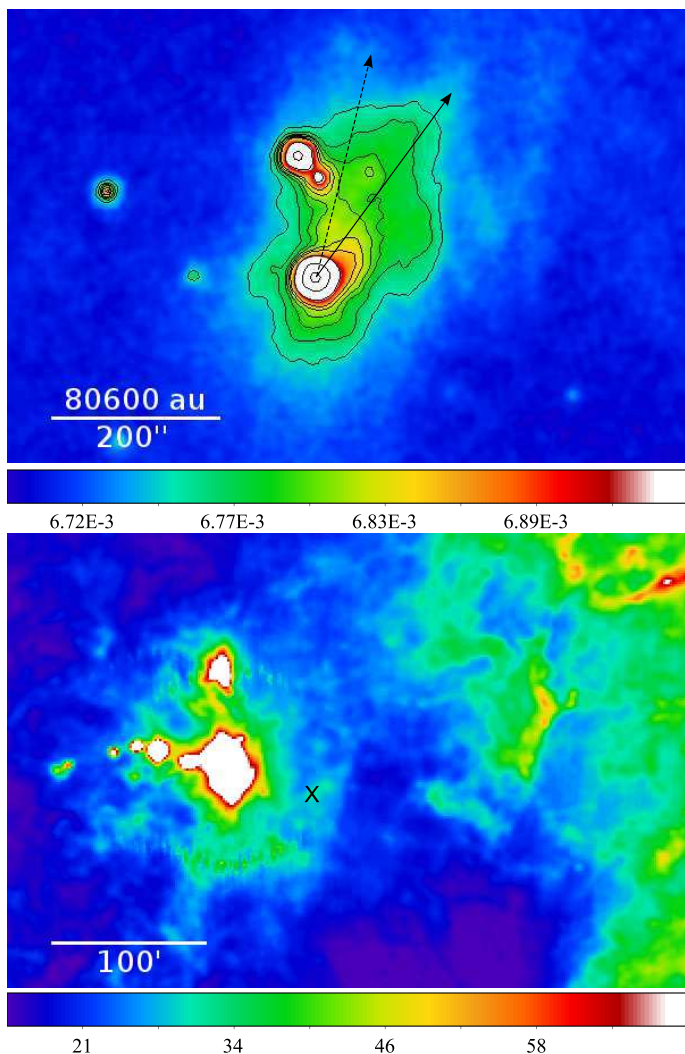
Fig. 9. *Upper panel:* WISE W4 image of V696 Mon at 22 μm. The continuous black arrow gives the uncorrected proper motion from the reprocessed Hipparcos catalogue (van Leeuwen 2007), while the dashed arrow points to the direction of the space motion corrected from the solar motion (Coşkunoğlu et al. 2011). The colour bar values are given in Jy pix^{-1}. *Lower panel:* IRAS 100 μm image of the surroundings of V696 Mon (marked as an X). The colour bar values are given in MJy sr^{-1}.

For those, we used the distance of the star to the bow shock to derive the mass loss rate of the matter that escapes from the system. For both systems we estimate a mass-loss rate of $\approx 10^{-9}\ M_\odot$ yr^{-1}, which is comparable to the mass loss rate found for single B-type stars and much lower than the predicted systemic mass-loss rate from the hotspot scenario ($\sim 10^{-5}\ M_\odot$ yr^{-1}, van Rensbergen et al. 2011; Deschamps et al. 2013, 2015). Incidentally, several bow shocks have been reported around single Be stars by e.g. Kobulnicky et al. (2012), Peri et al. (2012, 2015), and Noriega-Crespo et al. (1997). It seems therefore most likely that the bow shocks reported here are unrelated to the binary nature of the considered Be stars, and are of the same origin as those observed among non-binary Be stars. However, this does not entirely exclude the existence of systemic mass loss in these systems. It could well be that the mass transfer episode has already come to an end and the systemic mass loss rate has dropped.

Therefore, the prospects of finding observational support for systemic mass loss in Algols seem dark. Of the initial sample of 70 targets, only a handful of stars appear to exhibit IR excesses (see Figs. 1–5 and Figs. 13-14 of D15). It is conceivable that the simulations of D15 overestimate the amount of dust which survives the hotspot mechanism. For the two stars which show presence of circumstellar material expressed by a bow shock (π Aqr and φ Per), both shocks do not appear to be tied to systemic mass loss.

In the case of CX Dra, we were not able to identify the shaping mechanism responsible for the asymmetric circumstellar emission. Both common triggers for asymmetries, ISM interaction forming a bow shock and binary interaction forming an Archimedean spiral, can be excluded for various reasons. We note therefore that this system is an interesting case for further observations, since it may be a case where mass lost from the system is visible in the circumstellar environment.

References

Baranov, V. B., Krasnobaev, K. V., & Kulikovskii, A. G. 1971, Soviet Physics Doklady, 15, 791
Berdyugin, A. & Piirola, V. 2002, A&A, 394, 181
Bjorkman, K. S., Miroshnichenko, A. S., McDavid, D., & Pogrosheva, T. M. 2002, ApJ, 573, 812
Brancewicz, H. K. & Dworak, T. Z. 1980, Acta Astron., 30, 501
Budding, E., Erdem, A., Çiçek, C., et al. 2004, A&A, 417, 263
Chaubey, U. S. 1979, Ap&SS, 64, 177
Coşkunoğlu, B., Ak, S., Bilir, S., et al. 2011, MNRAS, 412, 1237
Collins, II, G. W. 1987, in IAU Colloq. 92: Physics of Be Stars, ed. A. Slettebak & T. P. Snow, 3–19
Comeron, F. & Kaper, L. 1998, A&A, 338, 273
Cox, N. L. J., Kerschbaum, F., van Marle, A.-J., et al. 2012, A&A, 537, A35
Crawford, J. A. 1955, ApJ, 121, 71
de Bruijne, J. H. J. & Eilers, A.-C. 2012, A&A, 546, A61
Dehnen, W. & Binney, J. J. 1998, MNRAS, 298, 387
Deschamps, R., Braun, K., Jorissen, A., et al. 2015, A&A, 577, A55
Deschamps, R., Siess, L., Davis, P. J., & Jorissen, A. 2013, A&A, 557, A40
Draine, B. T. 1981, ApJ, 245, 880
Draine, B. T. 1985, ApJS, 57, 587
Dunstall, P. R., Fraser, M., Clark, J. S., et al. 2012, A&A, 542, A50
Gies, D. R., Bagnuolo, Jr., W. G., Ferrara, E. C., et al. 1998, ApJ, 493, 440
Hanuschik, R. W., Hummel, W., Sutorius, E., Dietle, O., & Thimm, G. 1996, A&AS, 116, 309
Harmanec, P. 2001, Publications of the Astronomical Institute of the Czechoslovak Academy of Sciences, 89, 9
Hummel, W. & Štefl, S. 2001, A&A, 368, 471
Johnson, D. R. H. & Soderblom, D. R. 1987, AJ, 93, 864
Jorissen, A., Mayer, A., van Eck, S., et al. 2011, A&A, 532, A135
Kobulnicky, H. A., Lundquist, M. J., Bhattacharjee, A., & Kerton, C. R. 2012, AJ, 143, 71
Lamers, H. J. G. L. M., Zickgraf, F.-J., de Winter, D., Houziaux, L., & Zorec, J. 1998, A&A, 340, 117
Linnell, A. P., Peters, G. J., & Polidan, R. S. 1988, ApJ, 327, 265
Maercker, M., Mohamed, S., Vlemmings, W. H. T., et al. 2012, Nature, 490, 232
Mastrodemos, N. & Morris, M. 1999, ApJ, 523, 357
Mayer, A., Jorissen, A., Kerschbaum, F., et al. 2011, A&A, 531, L4
Mihalas, D. & Binney, J. 1981, Galactic astronomy: Structure and kinematics /2nd edition/
Noriega-Crespo, A., van Buren, D., & Dgani, R. 1997, AJ, 113, 780
Peri, C. S., Benaglia, P., Brookes, D. P., Stevens, I. R., & Isequilla, N. L. 2012, A&A, 538, A108

Peri, C. S., Benaglia, P., & Isequilla, N. L. 2015, A&A, 578, A45

Porter, J. M. & Rivinius, T. 2003, PASP, 115, 1153

Sarna, M. J. 1993, MNRAS, 262, 534

Snow, Jr., T. P. 1981, ApJ, 251, 139

Ueta, T., Speck, A. K., Stencel, R. E., et al. 2006, ApJ, 648, L39

van Buren, D. & McCray, R. 1988, ApJ, 329, L93

van Leeuwen, F. 2007, A&A, 474, 653

van Rensbergen, W., de Greve, J. P., Mennekens, N., Jansen, K., & de Loore, C. 2011, A&A, 528, A16

Weaver, R., McCray, R., Castor, J., Shapiro, P., & Moore, R. 1977, ApJ, 218, 377

Wilkin, F. P. 1996, ApJ, 459, L31

Wright, E. L., Eisenhardt, P. R. M., Mainzer, A. K., et al. 2010, AJ, 140, 1868

Zharikov, S. V., Miroshnichenko, A. S., Pollmann, E., et al. 2013, A&A, 560, A30

Appendix A: List of objects

Table A.1. 70 Algols and Algol-like Be stars with a WISE source counterpart sorted by declination. Objects marked with an asterisk (*) show extended emission in WISE W4, while the plus (+) sign marks objects with a WISE W4/W1 flux ratio which is above the blackbody law (see Tab. 6 in D15). References: (1): Harmanec (2001); (2): Brancewicz & Dworak (1980); (3): Budding et al. (2004).

V* Name	2MASS	HD/BD	Spec. type	Ref.
BP Mus	J12503772-7146186			3
DW Aps	J17233003-6755448	HD 156545	B6III	2,3
EP TrA	J15492615-6415574	HD 140809	A0	2,3
AN Tuc	J23302225-5825346	HD 221184	A5III	2,3
R Ara		HD 149730	B9IV	1,2,3
UZ Nor +	J16281156-5319215		B?	3
V646 Cen	J11365877-5312354	HD 100987	B8IV	2,3
RV Pic	J04572970-5208458	HD 32011	A1V	2,3
CZ Vel *+	J09104446-5042405		B3	3
KV Pup	J07471912-4832122	HD 63562	A0IV	2,3
TT Hor	J03270438-4552566			3
DN Vel	J09193768-4540477	HD 80692	A0III	2,3
VY Mic	J20490707-3343543	HD 198103	A4III	2,3
DM Pup	J08070409-2531522		A2.5	3
AA Pup	J08013612-2443034	HD 66226	F3IV	2,3
YY CMa	J07005186-1914315		A2V	3
AO Eri	J04320093-1744475		A2	2,3
SS Lep +	J06045913-1629039	HD 41511	A1V	1
W Ser +	J18095070-1533009	HD 166126	F5III	1,2,3
RY Sct +	J18253147-1241241	HD 169515	O9.7Ibep	1,2,3
XY Pup		HD 67862	A3	1,2,3
V644 Mon	J06570938-1049281	HD 51480	Ape	1
AW Mon		BD-10 2233	A2	2,3
RZ Sct	J18263352-0912060	HD 169753	B3Ib	1,2,3
XZ Aql	J20221335-0721034	HD 193740	A2	2,3
V696 Mon *+	J06041349-0642321	HD 41335	B2Vne	1
AR Mon	J07204845-0515357	HD 57364	K0II	2,3
AU Mon	J06545471-0122328	HD 50846	B4IV	1,2,3
V509 Mon +	J06471071-0102147		G4IV	3
π Aqr *+	J22251662+0122389	HD 212571	B1Ve	1
AC Tau	J04370635+0141311		A8	2,3
SS Cet		HD 17513	A2	2,3
AX Mon	J06303293+0552012	HD 45910	B2III	1
DN Ori	J06002835+1013049	HD 40632	A2e	1,2,3
FM Ori	J05085439+1033341	HD 241071	A5	3
V930 Oph	J18414565+1202111			3
BI Del	J20273862+1420091		G0	2,3
AL Leo	J09581290+1817282		F5	2,3
U Sge	J19184840+1936377	HD 181182	B7.5V	1,2,3
AL Gem	J06573855+2053325	HD 266913	F6V	2,3
RS Vul	J19174000+2226284	HD 180939	B5V	2,3
			Continued on next column	

V* Name	2MASS	HD/BD	Spec. type	Ref.
DH Her +	J18473455+2250458	HD 343047	A5	2,3
RW Tau	J04035432+2807334	HD 25487	B8Ve	1,2,3
U CrB	J15181133+3138492	HD 136175	B6V	1,2,3
BC Aur	J05461654+3250500			3
RX Gem	J06501154+3314207	HD 49521	A0	1,2,3
CG Cyg	J20581343+3510298		G9.5V	2,3
V367 Cyg +	J20475958+3917156	HD 198288	A3Ibep	1,2
AB Per	J03374520+4045494	HD 275604	A5	2,3
SX Aur *+	J05114292+4209553	HD 33357	B1Vne	1,2,3
RW Per	J04201676+4218517	HD 276247	A2	1,2,3
TX UMa	J10452050+4533586	HD 93033	B8V	1,2,3
GK And	J23534719+4534458			3
V995 Cyg	J19483443+4613424		B8	3
SW Cyg	J20065793+4617581	HD 191240	A2	1,2,3
IM Aur	J05152973+4624214	HD 33853	B9	2,3
RY Per	J02454210+4808379	HD 17034	B8V	1,2,3
KX And	J23070621+5011324	HD 218393	B3pe	1
φ Per *+	J01433964+5041192	HD 10516	B1.5Ve	1
AY Per	J03102513+5055543	HD 232756	B9	2,3
CX Dra *+	J18464309+5259166	HD 174237	B2.5Ve	1,3
V442 Cas +	J23401479+5357339		A0	3
SX Cas	J00104207+5453293	HD 232121	B5	1,2,3
DM Per	J02255800+5606099	HD 14871	B5V	2,3
GG Cas		BD+55 274	B5	2,3
RX Cas	J03074573+6734387		A5III	2,3
XY Cep	J23523291+6856015		B8	2,3
SS Cam	J07162474+7319570		G1III	2,3
XZ Cam	J05171266+7550053		A0	2,3
RS Cep	J05060320+8014524		A5III	1,2,3
TY UMi	J15175751+8351340	HD 138818	F0	3